



# Spark plasma sintering of Al–SiC composites with high SiC content: study of microstructure and tribological properties

Beata Leszczyńska-Madej<sup>1</sup> · Marcin Madej<sup>2</sup> · Anna Wąsik<sup>1</sup> · Dariusz Garbiec<sup>3</sup>

Received: 12 June 2023 / Revised: 1 August 2023 / Accepted: 17 August 2023 / Published online: 28 August 2023  
© The Author(s) 2023

## Abstract

The article presents the results of the microstructure and tribological properties of Al– $x$ SiC composites ( $x = 70$  and 90 wt% SiC) produced in spark plasma sintering (SPS). Due to their attractive thermal, physical, and mechanical properties, aluminum matrix composites with high-volume fractions of silicon carbide ( $> 50\%$ ) have become a major area of interest as a potential material for multifunctional electronic packaging and cryogenic applications. The SPS process was carried out in a vacuum atmosphere under various conditions. Composites with a density close to theoretical (96–98%) were obtained. X-ray diffraction and scanning electron microscopy with EDS analysis were used to characterize the microstructure. Mechanical properties were determined by hardness measurements and a three-point bending test. The tribological properties of the composites were determined utilizing a block-on-ring tribotester. As a criterion for wear resistance, weight loss measured under specific friction conditions, that is, depending on the type of material and the applied load, was adopted. The researched materials were characterized by an even distribution of the carbide phase in the matrix. Composites with the highest SiC phase content (90 wt%) had higher hardness (2537 HV1) and flexural strength ( $242 \pm 15$  MPa) with worse wear resistance at the same time. The weight loss of this composite was 0.43 and 0.76% for friction under loads of 100 and 200 N, respectively, and was 360 and 270% higher than that determined for the composites with the lower content of the SiC phase (70 wt%). The wear rate was three times higher for the Al-90wt%SiC composites.

**Keywords** Al–SiC composites · Spark plasma sintering · X-ray analysis · Scanning electron microscopy · Tribological properties · Wear mechanisms

## 1 Introduction

Due to their attractive thermal, physical, and mechanical properties, such as low thermal expansion, high thermal conductivity, low density and high specific stiffness, aluminum matrix composites with high-volume fractions of silicon carbide ( $> 50\%$ ) have become a major area of interest as a potential material for multifunctional electronic packaging and cryogenic applications [1]. This type of composites is also widely used in the aerospace, energy, transportation and precision instrument industries [2]. On one hand, the introduction of a high amount of SiC particles increases the areas of the matrix–reinforcement interface, and also increases the dislocation density in the material due to the difference in the thermal expansion coefficients between the metal and the ceramic [3]. On the other hand, in the case of a high content of reinforcing phase, wetting problems may arise [4, 5]. The compaction of composites with a reinforcing phase content exceeding 50 vol.% is a challenge due to the tendency

✉ Beata Leszczyńska-Madej  
bleszcz@agh.edu.pl

Marcin Madej  
mmadej@agh.edu.pl

Anna Wąsik  
anna.wasik@agh.edu.pl

Dariusz Garbiec  
dariusz.garbiec@pit.lukasiewicz.gov.pl

<sup>1</sup> Faculty of Non-Ferrous Metals, AGH University of Science and Technology, 30 Mickiewicza Ave., 30-059 Krakow, Poland

<sup>2</sup> Faculty of Metals Engineering and Industrial Computer Science, AGH University of Science and Technology, 30 Mickiewicza Ave., 30-059 Krakow, Poland

<sup>3</sup> Łukasiewicz Research Network – Poznań Institute of Technology, 6 Ewarysta Estkowskiego St, 61-755 Poznan, Poland

of ceramic particles to agglomerate (particularly for small particles of reinforcing phase) and porosity present in the agglomerated reinforcement. In turn, it is well known that the final properties of the composites are strongly dependent on the quality of the matrix–reinforcement interface that in turn is affected by the wettability between the matrix and the reinforcement, which can be improved at elevated temperatures [6]. However, at elevated temperatures, there is a probability that the reaction between Al and, SiC will occur and as a result, a detrimental  $Al_4C_3$  phase will form, which is thermodynamically unstable and can degrade the properties of the composites [7, 8].

One of the methods of obtaining Al–SiC composites that allow the effective control of negative interfacial reactions is spark plasma sintering (SPS). The SPS ensures a short holding time at low temperatures and limits grain coarsening [9, 10], provides appropriate densification and a microstructure devoid of micropores [11, 12]. Joule heating and plastic deformation lead to the high densification of Al–SiC composites with good interfacial bonding [13]. The presence of a liquid and a solid phase allows the formation of a strong bond in the metal–ceramic interphase, and the short contact time between the particles prevents the formation of intermetallic phases [14]. Therefore, SPS provides consolidated metal matrix composites improved mechanical, thermal and physical properties [15, 16].

Yu Hong et al. [17] investigated the interface microstructures of SiCp/6061Al composites with 50 vol.% SiC consolidated by SPS. They found that phases other than SiC and Al were not present in the microstructure of materials sintered in the temperature range of 480–530 °C. Hot pressing (HP) for the fabrication of high-volume SiCp/6061Al composites was used by Jian Sun et al. [18]. SiC particles were introduced in the amount of 50 vol.%. While at the sintering temperature of 630 °C, the composites exhibited strong bonding at the SiCp/Al interface, at the temperature of 640 °C and higher, the authors observed that an SiCp/Al interface reaction occurred and generated a typical reaction product of  $Al_4C_3$ . Ali Alizadeh et al. [19] compared the combined stir and squeeze casting methods in the fabrication of SiCp/Al5083 composites reinforced with 20, 25 and 30% SiC to examine their influence on the final properties. They concluded that the combined casting method allowed decreased porosity and better SiC particle distribution, and thus improved the compressive strength, hardness, and wear resistance. Authors of work [20] investigated the influence of the SiC reinforcement volume fraction on the wear properties. They concluded that the wear rate decreased with the volume, whereas the coefficient of friction increased. Gosh et al. [21] stated that the wear rate fell due to the increment in the volume fraction of SiC in LM6 Al-based composites produced by stir casting. The results concerning Al–SiC composites and presented in [22] by Smrutiranjana et al. show that the wear rises with the applied load, and the

wear mechanism might also change during friction. There are many papers devoted to the study of the tribological properties of aluminum matrix composites reinforced with ceramic particles (AMCs). However, only a few papers deal with the tribological properties of composites with a reinforcing phase content of more than 50 wt%. Earlier investigations of authors concerning Al–SiC composites with a high amount of SiC phase found that the coefficient of friction of composites with the 50 wt% SiC content was usually higher than that for the compacts with the 70 wt% SiC content, which resulted from the role of the Al matrix in the friction process. The presence of Al in the friction pair changed the mechanism that occurs there; the role of adhesion increased and influenced the growth in the coefficient of friction. Furthermore, the increase in the compression pressure applied during SPS has adverse effects on the coefficient of friction [23].

The selected findings presented demonstrate that appropriate selection of the manufacturing technology and process parameters, which allow a high degree of composite density to be achieved, will be important from the point of view of the final properties of composite materials reinforced with a high volume of fraction of reinforcement [24].

At present, there are few studies [4, 5, 23] on the production of Al–SiC composites with a high content of reinforcing phase, exceeding 50 wt%, by the SPS. The critical role in this type of composites is played by the interface between the aluminum matrix and SiC. In the case of a high content of the reinforcing phase, problems with wetting may occur. At the phase boundary, the  $Al_4C_3$  phase may also appear, which affects the properties of the composites. The data presented in the literature mainly concern the study of the thermal properties of such composites produced by various technologies [4, 6, 13, 17, 18]; there is no comprehensive information on the tribological properties of such composites, in particular on the content of the reinforcing phase exceeding 70 wt% and produced via the SPS. The analysis of data available in the literature was the motivation to take up this topic; a number of experiments were carried out regarding selection of the conditions of the SPS of composites with carbide phase contents of 70 and 90 wt%. Subsequently, using the optimized conditions, the composites were produced and their phase and microstructural characteristics were assessed, as well as their behavior in the friction pair under the conditions of technically dry friction.

## 2 Materials and methods

### 2.1 Materials and production process

The powders used in the study were air-sprayed aluminum grade 1070 (Benda Lutz, Skawina, Poland), with a particle size of less than 63  $\mu\text{m}$  and SiC powder (Karbtorund,

Poland) with a particle size in the range 60–80  $\mu\text{m}$ . The aluminum powder consisted of the following fractions: above 63  $\mu\text{m}$ —5%, in the range of 32–63  $\mu\text{m}$ —45–70%, the rest—below 32  $\mu\text{m}$ . Composites containing 70 and 90 wt% SiC were produced. The powder mixtures were mixed in a Turbula T2F mixer (WAB, Switzerland) for 1 h, then spark plasma sintered using an HP D 25/3 furnace (FCT Systeme, Germany). The size of the sintered samples was 40 mm in diameter and 10 mm in height. The parameters of the SPS are listed in Table 1, and Fig. 1 shows the sintering curves for the optimized conditions. In the case of the variant with 70 wt% SiC, a plateau of the shrinkage curve was observed, which proves the complete densification of the powder mixture under the optimized sintering conditions. Nevertheless, in the case of the variant with 90 wt% SiC, the plateau was not observed, which results from the upsetting of graphite punches at the temperature of 2100  $^{\circ}\text{C}$  and the compaction pressure of 100 MPa. Preliminary sintering experiments were performed at various temperatures. The temperature of the composites with the SiC content up to 70 wt% was the same as for aluminum or AMCs. When the SiC content was 90 wt%, the sintering behavior was close to the sintering of SiC, which is why a temperature of 2100  $^{\circ}\text{C}$  was needed to obtain high densification. At lower temperatures, the densification was significantly lower—below 90%.

The morphology of the powder particles used to produce the composites is shown in Fig. 2.

## 2.2 Microstructure characterization

The specimens for the microscopic examinations were embedded in conductive PolyFast resin, and then the thus prepared specimens were ground on abrasive papers with the following gradation: 220, 500, 800, 1200, 2000 and 4000, and two-stage mechanical polishing in accordance with the Struers procedure using a suspension of Dia Duo diamond paste with a grain size of 3  $\mu\text{m}$  and a colloidal suspension of silicon oxide OPS for finishing polishing with a grain size of  $\frac{1}{4}$   $\mu\text{m}$ . The microstructure of the composites was examined using a SU-70 (Hitachi, Japan) Schottky-type electron gun scanning electron microscope (SEM) with a NORAN System 7 (Thermo Scientific, USA) X-ray microanalysis system (EDS). The micrographs were taken during operation of the secondary electron (SE) and backscattered electron (BSE) detector. Accelerating voltage was used: 5 kV for observation of the powders and the microstructure of the composites, 10 kV for observation of the fractures after the three-point bending test, and 10 and 15 kV for observation of the surface after friction. The chemical composition tests were performed at an accelerating voltage of 15 kV. The phase composition was analyzed by means of a D8 Advance (Bruker, Germany) X-ray diffractometer with  $\text{Co K}\alpha = 1.79 \text{ \AA}$  cobalt lamp.

**Table 1** Parameters of spark plasma sintering (SPS) process

Sample	Temperature ( $^{\circ}\text{C}$ )	Heating rate ( $^{\circ}\text{C}/\text{min}$ )	Holding time (min)	Compaction pressure (MPa)
Al-70wt%SiC	600	RT–550 $^{\circ}\text{C}$ (100 $^{\circ}\text{C}/\text{min}$ ) 550–600 $^{\circ}\text{C}$ (25 $^{\circ}\text{C}/\text{min}$ )	20	100
Al-90wt%SiC	2100	RT–1950 $^{\circ}\text{C}$ (100 $^{\circ}\text{C}/\text{min}$ ) 1950–2050 $^{\circ}\text{C}$ (50 $^{\circ}\text{C}/\text{min}$ ) 2050–2100 $^{\circ}\text{C}$ (25 $^{\circ}\text{C}/\text{min}$ )	20	100

RT room temperature

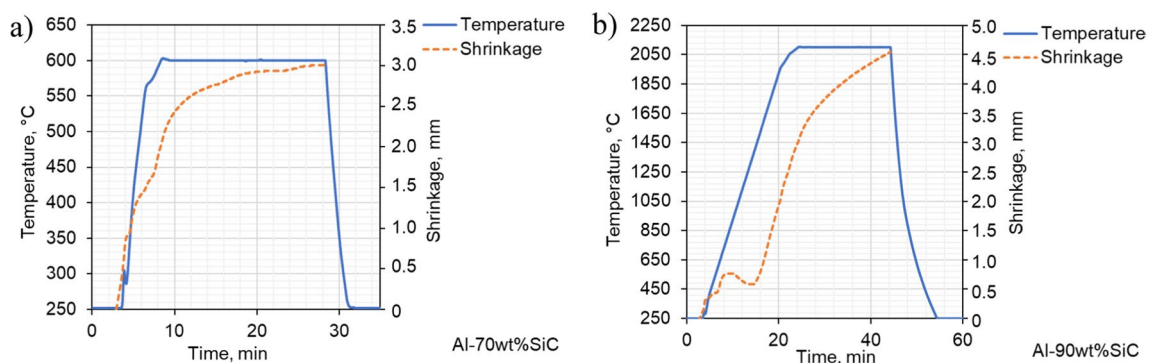
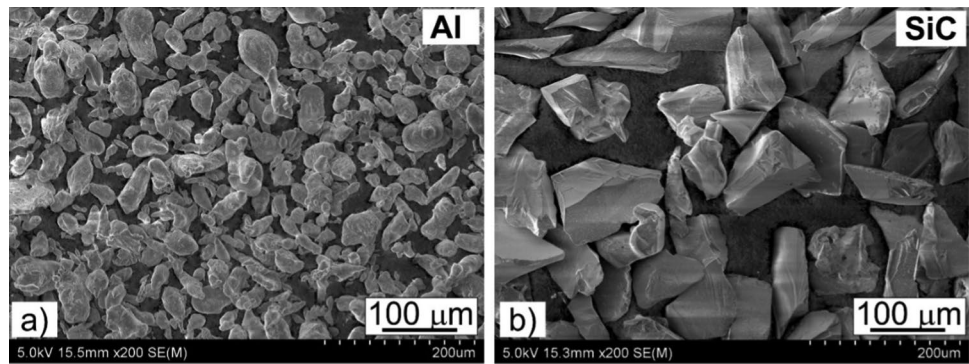


**Fig. 1** Shrinkage curves of: **a** Al-70wt%SiC, **b** Al-90wt%SiC

**Fig. 2** SEM micrographs of powders: **a** Al (<math>< 63 \mu\text{m}</math>), **b** SiC (60–80  $\mu\text{m}</math>)$



### 2.3 Physical and mechanical properties

The relative density of the composites was measured by the Archimedes method in accordance with the ISO 18754 standard. The theoretical density of the sinters was determined from the rule of mixtures, taking into account the initial contents of the individual phases for calculations. After comparison with the actual density determined by the Archimedes method, approximate values of relative density, and thus porosity were obtained.

The composite hardness was measured employing the Vickers method applying a load of 9.8 N in accordance with the ISO 6507-1 standard. The flexural test was conducted using a Z020 (Zwick Roell, Ulm, Germany) universal testing machine at a constant strain rate of 0.05 mm/s via the three-point bending test. The test was carried out on bars with dimensions of  $4 \times 4 \times 40$  mm cut from SPSeD samples. The tests were performed in accordance with the ISO 7438 standard. The fracture surfaces from the flexural test were examined by SEM.

### 2.4 Tribological properties

The tribological properties were tested utilizing a T-05 (Łukasiewicz – ITeE, Poland) block-on-ring tribotester (Fig. 3) at ambient temperature under technically dry friction conditions. A minimum of three tribological tests were performed for each variant of the studied material. During the test, a rectangular tribological specimen was mounted in a holder equipped with a hemispherical insert ensuring proper contact between the tested specimen and the steel ring rotating at a permanent speed. The friction surface ( $F$ ) of the specimen was perpendicular to the load ( $L$ ) direction. A double lever system was used to push the specimen toward the ring with a loading accuracy of  $\pm 1.5\%$ . The wear test conditions are listed in Table 2.

Prior to the test, the specimens were prepared according to the surface quality (a suitable roughness—less than  $1 \mu\text{m}$ ) and thoroughly degreased by washing with a Struers degreasing agent; after drying, they were weighed and

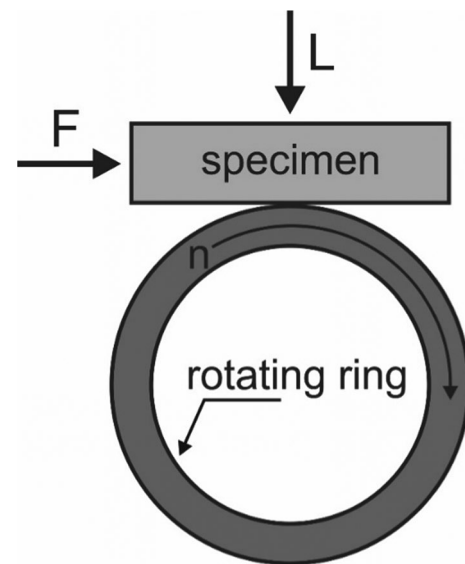


**Fig. 3** Diagram of T-05 block-on-ring tribotester;  $L$  load perpendicular to the friction surface,  $F$  friction force measurement

tested immediately thereafter. After the test, the specimen was washed, dried, and weighed. The weight loss was determined by the difference in weight. Since the initial specimens were characterized by different weights, in order to accurately characterize the differences, the weight losses were converted to %. The change in the coefficient of friction over time was determined for the whole test (1000 m). The load and friction force required to calculate the coefficient of friction were measured. To determine the wear mechanisms, the wear surface was analyzed by scanning electron microscope.

## 3 Results and discussion

### 3.1 Microstructure of composites

One of the main factors determining the homogeneous distribution of the strengthening phase in the matrix of



**Table 2** Wear test conditions

No.	Parameter	Value, unit
1	Dimensions of tested specimens	20×4×4 mm
2	Rotating ring	Heat-treated steel 100Cr6, 55 HRC, Ø49.5×8 mm
3	Rotational speed	136 rpm
4	Velocity	0.25 m/s
5	Sliding distance	1000 m
6	Sliding condition	Without lubricant (technically dry friction)
7	Ambient temperature	20 °C
8	Load	100 N, 200 N

composites is the ratio of the size of the matrix particles to the size of the reinforcement particles. A small difference in the size of the matrix and reinforcement particles allows a more uniform distribution of the reinforcing phase in the matrix. SiC powders with a size of 60–80  $\mu\text{m}$  and aluminum powders with a particle size of less than 63  $\mu\text{m}$  were used to produce the composites. This particle size of the reinforcing phase powder prevents the formation of agglomerates, unlike the fine powders available on the market (below 10  $\mu\text{m}$ ). Thanks to this, the use of a Turbula-type mixer enables the production of composites characterized by a relatively

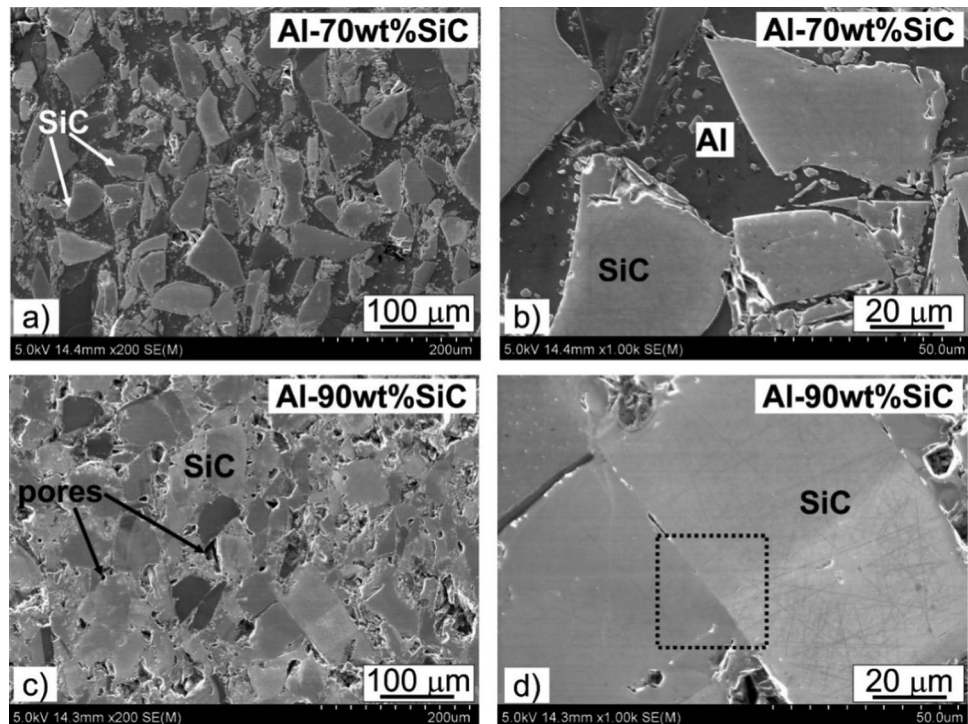
homogeneous distribution of the matrix against the background of particles of the reinforcing phase.

Figure 4 presents the microstructure of the investigated composites, taken at different magnifications using a scanning electron microscope, while Fig. 5 displays the maps of the distribution of elements. In the case of the composite with the lower content of the reinforcing phase (70 wt%), the particles of the hard SiC phase are evenly distributed in the plastic aluminum matrix. The SiC particles were partially crushed as a result of the SPS; numerous small SiC particles are visible in the microstructure. No discontinuities were found at the SiC-plastic aluminum matrix boundary (Figs. 4a, 5a). In the case of the composites containing 90 wt% SiC, SiC particles are visible in the microstructure, aluminum is present between the SiC particles, and pores are also present locally. Areas containing only the ceramic phase are visible in the microstructure. A good connection was found between the SiC particles and between the aluminum matrix and the ceramic reinforcement (Figs. 4b, 5b). In addition, alumina particles are observed in the microstructure, which are located mainly on the boundaries of the aluminum grains (Fig. 5).

### 3.2 XRD analysis

Phase composition studies performed by X-ray diffraction revealed the presence of the following phases in the examined composites: SiC, Al,  $\text{Al}_2\text{O}_3$ , as well as  $\text{SiO}_2$ , Si and  $\text{Al}_4\text{C}_3$ , with the peaks from the Si and  $\text{Al}_4\text{C}_3$  phases

**Fig. 4** Microstructure of spark plasma sintered Al–SiC composites; SEM



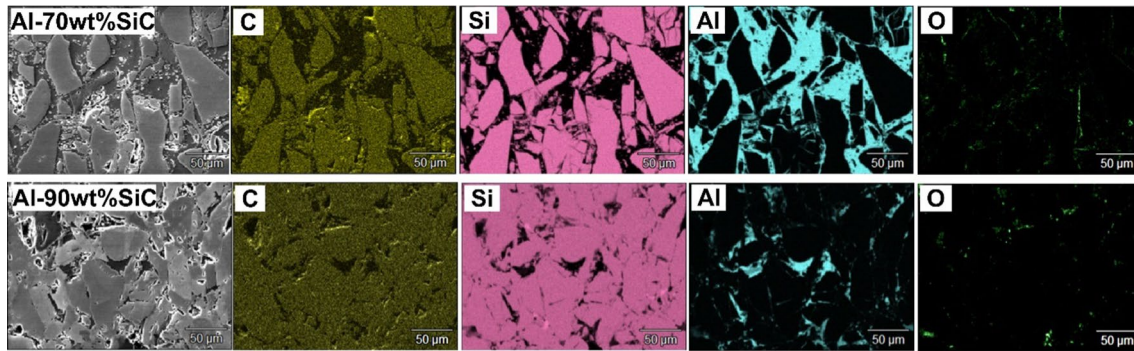


**Fig. 5** Microstructure and maps of distribution of elements: C, Si, Al, O; SEM

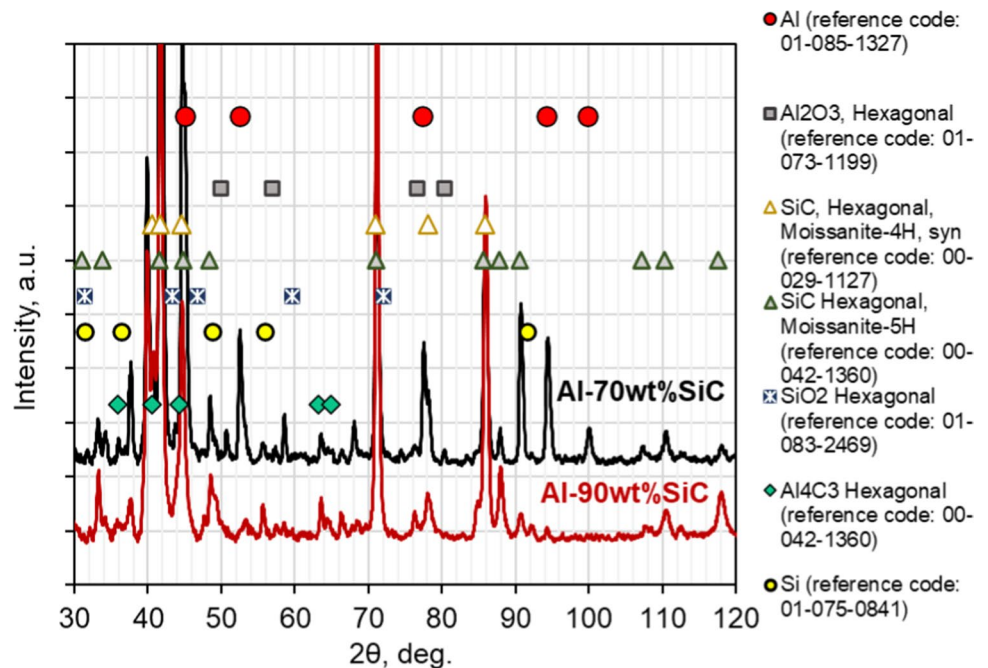
being more intense in the composite containing 90 wt% SiC (Fig. 6). The higher sintering temperature (2100 °C) favors the decomposition of SiC; as a result of the reaction free Si and  $\text{Al}_4\text{C}_3$  are formed. The reactions of aluminum carbide formation have been described, for example, in works [25–27] concerning cast Al–SiC composites. As a result of contact between liquid aluminum and SiC particles, the brittle  $\text{Al}_4\text{C}_3$  compound and particles of free silicon are formed at the interface of these two phases, which adversely affect the mechanical properties. The reaction of aluminum carbide formation was observed already at a temperature of about 670 °C, just after exceeding the melting point of aluminum, and its identification was made on the basis of the heat released as a result of the reaction. Aluminum carbide is formed according to Reaction (1) [28]:



In the case of the SPS of composites with the lower content of the SiC phase, the explanation of the formation of  $\text{Al}_4\text{C}_3$  can be sought in the local increase in temperature as a result of both the impact of sparks on the surface of the particles and exothermic allotropic transformations of alumina during the SPS and the accompanying heat release, which is responsible for local melting of the aluminum matrix. Earlier work on Al–SiC composites, but with a lower SiC content, produced via the SPS, also proved the presence of aluminum carbide [29].

Aluminum has a strong affinity for oxygen, as a result of which the surface of the powder particles is covered with a thin layer of oxide, which is a barrier to the formation of a permanent intermetallic connection between the sintered particles, and it reacts with some ceramics

**Fig. 6** X-ray diffraction spectra of Al–*x*SiC (*x* = 70, 90 wt%)



to form intermetallic phases affecting the quality of the metal–ceramic connection, and thus the final properties of the composite [30]. The oxide film is continuous, thermodynamically stable, pore-free and prevents further oxidation of the aluminum. For this reason, a continuous layer of alumina can be treated as a positive aspect, which however, in the particular case, i.e. during sintering, acts as a barrier hindering the formation of metal–metal connections, necessary for the formation of necks between the particles, their growth, and hindering the volumetric diffusion processes responsible for shrinkage during the sintering process. The sintering temperature of alumina powder is much higher (by about 1000 °C) than aluminum-based powder [31, 32]. Therefore, the oxide layer must be broken or removed in order to ensure an effective sintering process. An advantage of sintering aluminum is the participation of the liquid phase, which violates the integrity of the oxide layer formed on the surface of the aluminum particles by penetrating the interface between the oxide layer and the metal [31]. The alumina covering the aluminum powder obtained by the sputtering process is usually amorphous. Nonetheless, it can undergo transformation when aluminum is heated, including its transformation into a crystalline form. There are two mechanisms that enable rupture of the continuous oxide layer, and thus lead to direct contact between the metallic aluminum and the surrounding gas atmosphere. One of them is the polymorphic transformation of alumina in the sintering process, and the other is the presence of thermal stresses generated by a large difference in the thermal expansion coefficients between aluminum and alumina [31, 33]. Alumina formed at low temperature is amorphous. Its thickness is usually 0.5–5 nm. When its critical thickness is exceeded due to further oxidation, the layer loses its stability and transforms into the crystalline variety  $\gamma$ -Al<sub>2</sub>O<sub>3</sub>. The structure of Al<sub>2</sub>O<sub>3</sub> changes from amorphous to crystalline  $\gamma$  under the influence of a temperature increase above 400 °C. Owing to the difference in the densities between amorphous alumina (3.05 g/cm<sup>3</sup>) and crystalline  $\gamma$ -Al<sub>2</sub>O<sub>3</sub> (3.66 g/cm<sup>3</sup>), the initially continuous layer breaks down, and thus does not completely cover the surface of the aluminum particles. The second mechanism leading to discontinuity in the oxide layer results from the stresses occurring during heating of the Al<sub>2</sub>O<sub>3</sub>/Al interface. The coefficient of thermal expansion of aluminum  $2.39 \times 10^{-5} \text{ K}^{-1}$  is about 10 times that of  $\gamma$ -Al<sub>2</sub>O<sub>3</sub>  $2.61 \times 10^{-6} \text{ K}^{-1}$ . Because of the large difference in the coefficients of thermal expansion during heating, the fracture toughness of alumina is easily exceeded. As a result, gases from the sintering atmosphere come into direct contact with the metallic aluminum [31]. The SPS, despite the fact that it is carried out in a vacuum atmosphere, does not lead to a complete reduction

of Al<sub>2</sub>O<sub>3</sub> [29], which is confirmed by the obtained results of the investigations presented in this paper.

### 3.3 Physical and mechanical properties

The density of the studied composites is 95.72–98.16% and is higher (close to theoretical) for the composite with the content of reinforcing phase of 90 wt%. The hardness of the composite with the content of reinforcing phase of 70 wt% is  $286 \pm 63 \text{ HV1}$ , while the composite with the content of reinforcing phase of 90 wt% is  $2537 \pm 226 \text{ HV1}$ . The significantly higher hardness of the composite with the 90 wt% SiC content results from the share and distribution of the aluminum matrix in the microstructure of these composites. The Vickers hardness measurement is carried out using a diamond pyramid, which, penetrating into the tested material with the 90 wt% content of silicon carbide, hits with high probability mainly a large carbide particle, giving a result similar to the hardness of pure carbide. The influence of the matrix, owing to its low content and relatively homogeneous distribution in the microstructure, is insignificant. The porosity present in the composites with the 90 wt% SiC content may also be of greater importance in the obtained result, as its share reaches about 4%. In those containing 70 wt% SiC, the matrix affects proportionally more hardness measurements in contrast to those containing 90 wt% SiC. The results of the flexural strength measurements proved the higher resistance of the composites with the higher content of the SiC reinforcing phase. The obtained results were  $198 \pm 5$  and  $242 \pm 15 \text{ MPa}$  for the Al-70wt% SiC and Al-90 wt% SiC composites, respectively (Table 3). This result can be explained by the good connection between the SiC particles, which is confirmed by the results of the microstructure observations (Figs. 4 and 5) and by the arrangement of the aluminum matrix, which is evenly located between the SiC particles. In the case of the composite with the lower content of SiC, the aluminum matrix occupies larger areas, which probably has a negative effect on the bending strength. The use of a higher content of the SiC reinforcing phase and a higher sintering temperature allowed composites to be obtained characterized by higher hardness and higher flexural strength, which was achieved by a greater concentration of particles of the reinforcing phase in the matrix, thus reducing the effective distance between the SiC particles,

**Table 3** Measurement results of physical and mechanical properties of studied composites

Samples	Relative density (%)	Hardness, HV1	Flexural strength (MPa)
Al-70wt%SiC	95.72 ± 0.5	286 ± 63	198 ± 5
Al-90wt%SiC	98.16 ± 0.5	2537 ± 226	242 ± 15



thanks to which these particles form a continuous skeleton, resulting in better strength properties.

The micrographs of the fractures after three-point bending presented in Fig. 7 have a transcrystalline ductile character within the aluminum matrix and a transcrystalline cleavable character within SiC. In both composites, the character of cleavage cracking predominates, and the share of ductile cracking is higher in the composite with the lower content of the SiC phase (70 wt%). The ductile transcrystalline fracture is characterized by the presence of numerous dimples, which indicate plastic deformation during bending of the aluminum matrix. Equally characteristic are the locally visible SiC particles partially covered with the matrix material, which proves the good cohesion of the matrix material and the reinforcing phase (Fig. 7c, f). In these places, the interface cohesion was retained.

### 3.4 Friction—wear properties

The results of the wear resistance tests of the researched composite materials are shown in Fig. 8. The weight loss recorded under specific friction conditions, i.e. depending on the type of material and applied load, was adopted as the wear resistance criterion. This approach makes it possible to classify materials in terms of their wear resistance under specific friction conditions and the adopted test method. The results presented in Fig. 8 clearly show that the composites with the lower content of silicon carbide (70 wt%) are characterized by much greater resistance to wear than the composites with the content of 90 wt% SiC, i.e. it is an inverse relationship to the hardness results obtained via the Vickers method. From the point of view of relative density, both

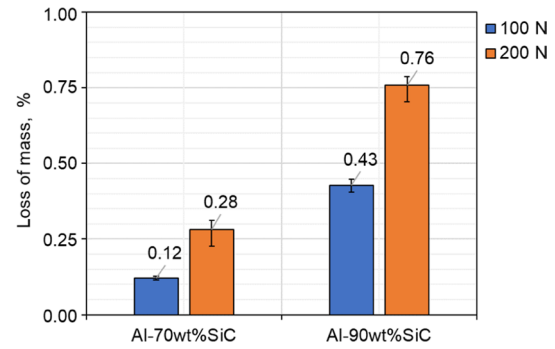


Fig. 8 Weight loss registered for studied composites

materials are characterized by a value above 95%, which allows the role of pores to be reduced in the friction process. The main factor determining the wear resistance will, therefore, be the share of the ceramic phase and the share and distribution of the matrix. Increasing the share of SiC particles in the friction pair, and locally the lack of matrix between these particles causes an increased tendency to chipping of SiC particle fragments, resulting from dynamic load changes in the friction pair and the tendency of ceramics to crack. This also results in the appearance of additional abrasive particles in the friction pair, adversely affecting the further course of the process. Doubling the load on the friction pair causes a significant increase in weight loss, but proportionally smaller in the case of the load of 200 N in the composites containing 90 wt% SiC compared to the composites containing 70 wt% SiC. Paradoxically, the increased load may have a positive effect on the wear rate resulting from chipping of the SiC particles through their mechanical

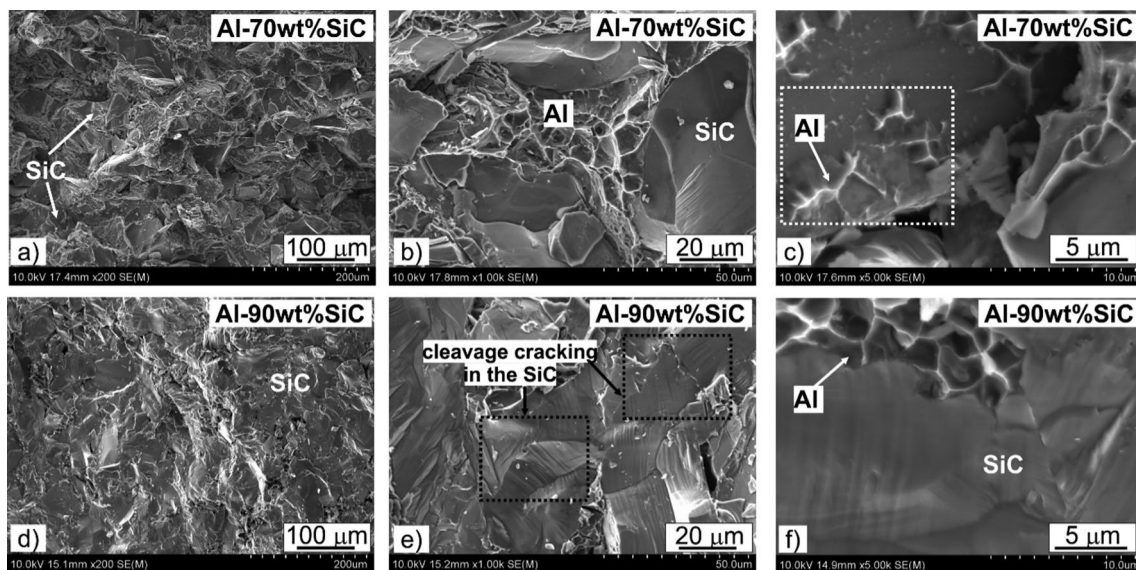


Fig. 7 Fractures of specimens after three-point bending



pressure, especially in the first stage of the test, in which the load is more concentrated on a smaller friction surface.

The wear rate of the investigated composites was also determined as (2):

$$W_r = \frac{\Delta m}{L * D} \left[ \frac{g}{N * m} \right], \tag{2}$$

where  $\Delta m = m_{\text{start}} - m_{\text{finish}}$  (g),  $L$  is the normal load (N), and  $D$  is sliding distance (m).

After taking into account the share of the reinforcing phase and the load, it was noticed that the wear rate for the composites containing 70 wt% SiC differs slightly, with increasing load causing a slight increase in  $W_r$ , while increasing the load in the steel-composite friction couple with 90 wt% SiC reduces the wear rate of this material compared to the 100 N load (Fig. 9).

On the basis of changes in the friction force measured continuously during the test on a sliding distance of 1000 m, the average coefficient of friction for the tested composites was determined, which is presented in Fig. 10. The investigated parameter strictly depends on the type of material and the applied load in the friction couple. Its change with increasing load is different for both the researched contents of SiC reinforcing phase. For the material containing 70 wt% of this carbide, greater pressure reduces the coefficient of friction, while for the content of 90 wt%, the coefficient rises slightly. In order to thoroughly analyze the phenomena occurring during the test, which may affect the coefficient of friction, the course of changes in the friction force depending on the test time was also presented, and the surface morphology after friction was observed. Figure 11a and b displays the course of friction force changes depending on the test time and SiC content.

The curves showing changes in the friction force as a function of time of the tribological test reveal a course consisting of two stages: run-in and proper friction. The time and course of the run-in stage depends primarily on the content of silicon carbide, and the value of the loading

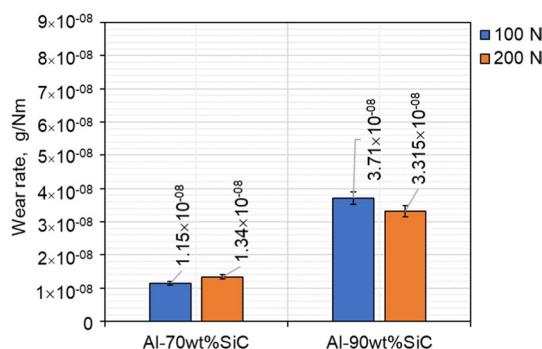


Fig. 9 Wear rate determined for studied composites in relation to sliding distance and applied load

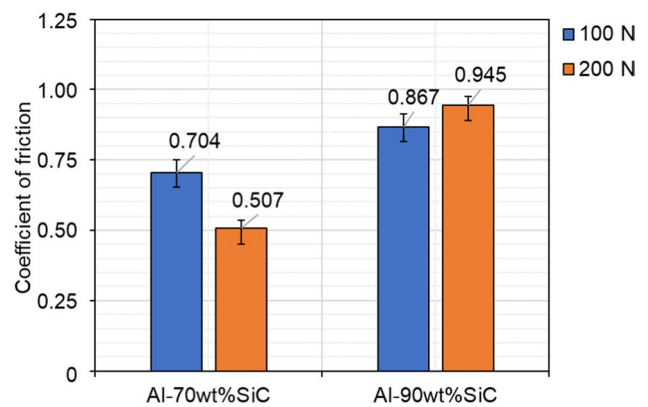


Fig. 10 Average coefficient of friction for studied composites

force also has an impact. For the composites containing 90 wt% SiC (approx. 170 s), the run-in time is shorter than in the test for the composites containing 70 wt% SiC (approx. 500 s). The amplitude of changes in the friction force, and thus also the coefficient of friction, in the first stage are much more intense in the case of the Al-90wt% SiC composites. After stabilizing the friction conditions, the course of force changes is relatively stable in all the cases, while a greater

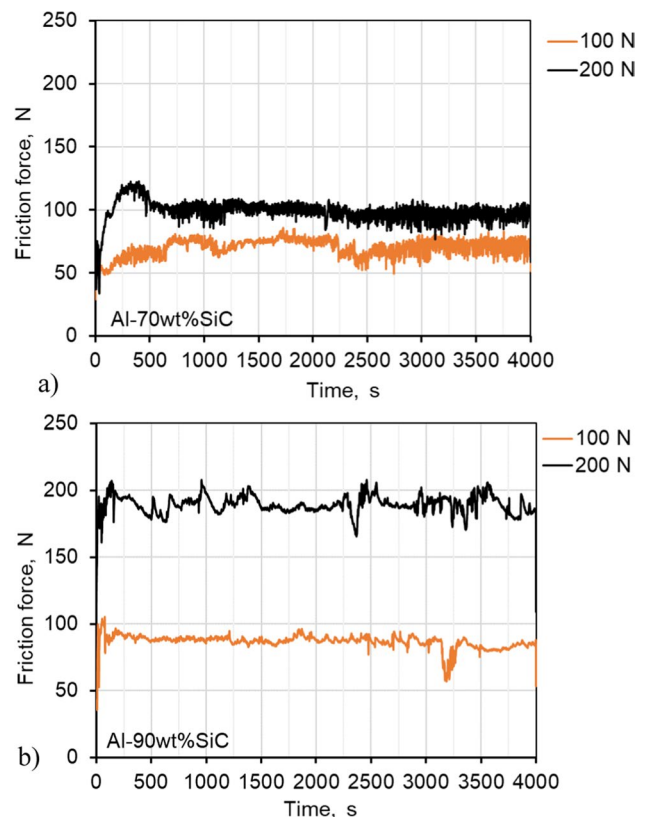
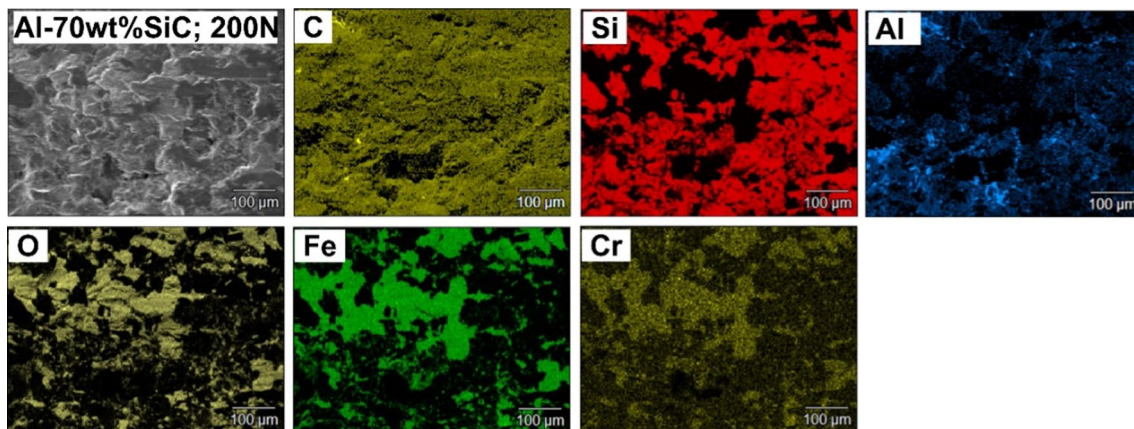
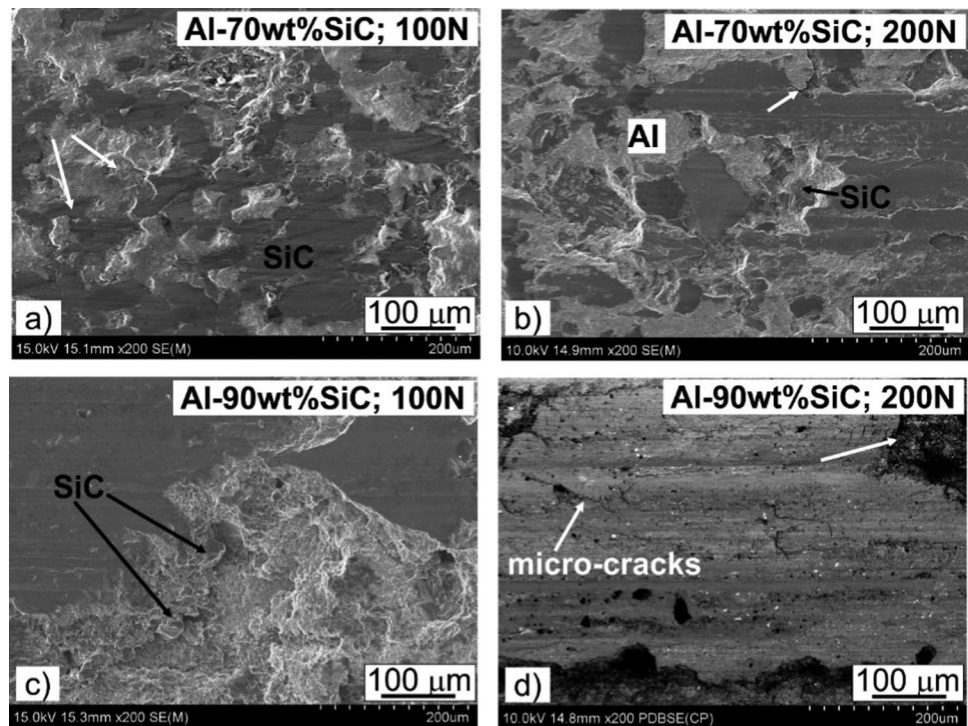


Fig. 11 Course of changes in friction force for composite: a Al-70wt% SiC, b Al-90wt% SiC

share of SiC favors temporary abrupt changes in force, which may result from possible chipping of the reinforcing phase or other friction mechanisms, verified by analyzing the surface morphology after sliding contact as shown in Figs. 12, 13, and 14. The chipping of the ceramic phase and abrasive mechanisms, which could be expected as dominant in this type of materials after the analysis of the morphology of the surface after friction, turned out to be marginal phenomena of the wear process, especially in the case of the composites with the content of 70 wt% SiC. Abrasive wear leading to the smoothing of mutually rubbing surfaces dominates in the run-in stage, giving way to other phenomena after this stage.

By analyzing the surfaces after friction presented in Fig. 12, it can be concluded that the basic mechanism observed after the friction process is the smearing of the matrix on the surface and moving in the direction of friction. One can also notice matrix stacking on the obstacles, i.e. the edges of the SiC particles. It is also possible to transfer the material of the steel counter-specimen to the surface of the examined specimens and simultaneously oxidize the surface, especially in the areas of the matrix and deposition, mainly iron from the counter-specimen. The presence of oxidation and chipping of the formed oxides may be evidenced by the chipping occurring especially on the accumulations

**Fig. 12** Surface morphology after sliding contact of composites: **a, b** Al-70wt% SiC (**a** 100 N load, **b** 200 N load), **c, d** Al-90wt% SiC (**c** 100 N load, **d** 200 N load)



**Fig. 13** Maps of distribution of elements (C, Si, Al, O, Fe, Cr) on surface after friction of Al-70wt% SiC specimen, load 200 N

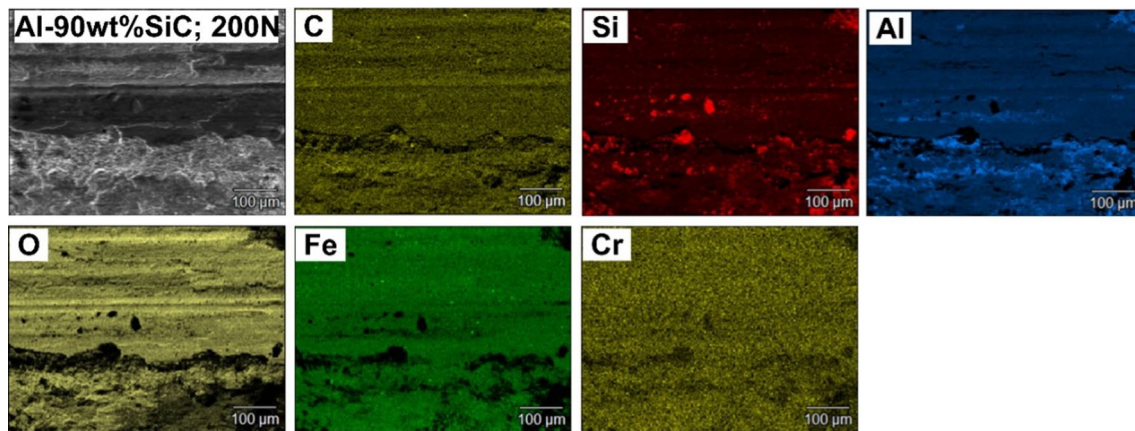


**Fig. 14** Maps of distribution of elements (C, Si, Al, O, Fe, Cr) on surface after friction of Al-90% SiC specimen, load 200 N

observed on the surface of the composite with the content of 70 wt% reinforcing phase after friction under the load of 100 N (Figs. 12a, 13). Increasing the share of the reinforcing phase does not significantly affect a change in the friction mechanism; one can clearly see the smearing of the matrix, filling the chippings present on the surface and its accumulation on the protruding edges of the SiC particles. However, the participation of this process on the surface is locally disproportionate to the content of the matrix in these composites (Figs. 12b, 14), which also proves the transfer of the counter-specimen material to the surface of the composites involved in friction. It can also be assumed that the matrix is locally transported over longer distances to fill the craters formed after SiC chipping, enabling the formation of purely ceramic surfaces exposed to dynamic load changes, and thus further chipping resulting in increased weight loss compared to the composites with the higher matrix content, which is, therefore, of greater importance during the sliding contact, partially eliminating the effects of load changes, seemingly "protecting" the ceramic particles from chipping.

The element distribution maps (Figs. 13, 14) confirmed the smearing of not only aluminum on the surface of the investigated composite, but also the strong transfer and adhesion of the counter-specimen material, mainly iron, to the surface of the composites. In addition, the analysis of the results of these tests clearly reveal oxidation of both the aluminum and iron debris, as well as chipping of the resulting oxides, which is indicated by numerous craters present on the surface. The presence of  $\text{Al}_2\text{O}_3$  in the form of fine particles in the friction pair may explain and confirm the mechanism of micro-crack formation on the SiC surface. The process of the interaction of the specimen with the counter-specimen is complex; several mechanisms operate in the sliding contact, depending on the work mechanisms, which is the reason why the wear rate of aluminum matrix composites exhibits non-linear characteristics [34, 35]. The

ceramic particles of the reinforcing phase are harder than the counter-specimen material, which removes the counter-specimen material and transfers it to the surface of the worn specimen. Fe particles are easily transformed into iron oxide particles as a consequence of interaction with oxygen contained in the atmosphere. Over a certain period of sliding, a layer of oxidized particles forms on the counter surface. The layer, known as the mechanical mixed layer (MML), has an effect similar to a solid lubricant. This facilitates easy sliding of the composite specimen [36]. The load-bearing SiC particles eventually pull out of the matrix or are fractured during sliding. The hard debris of these SiC particles was scattered along the sliding path along the counter surface. The debris enters the sliding contact space for each turning of the counter surface. This creates the situation that three bodies interact during sliding. Thus, the wear mechanism is changed to three-body friction [35, 37], which requires less force for sliding than two-body friction, because the debris on the contact surface reduces the effective contact area of the specimen.

## 4 Conclusions

This paper presents detailed studies on the characteristics, phase identification and tribological behavior of Al–SiC composites with a high content of the reinforcing phase of 70 and 90 wt% produced using the SPS under optimized conditions. The tests of the tribological properties were conducted in conditions of technically dry friction at room temperature, using loads of 100 and 200 N and a sliding distance of 1000 m. The main conclusions resulting from the investigations can be summarized as follows:

- In the case of the Al-70wt%SiC composite sintered at 600 °C, a plateau was observed on the shrinkage curve,



which indicates compaction of the powder mixture, and the obtained density is 95.72%. This is related to the sintering temperature typical for aluminum and Al-SiC composites with a content of the reinforcing phase in the range of 20–50 wt% SiC. On the other hand, in the case of the Al-90wt%SiC composite, no plateau was observed and the composite has a density of 98.16%.

- Sintering of the mixture with 70 wt% SiC at a temperature greater than 600 °C and a pressure of 100 MPa caused intensive aluminum flow, which led to destruction of the graphite die. On the other hand, the sintering of a mixture of Al with 90 wt% SiC at the temperature of 2100 °C and the compaction pressure of 100 MPa caused upsetting of the graphite punches, which made it impossible to observe the plateau of the shrinkage curve.
- A characteristic feature of the microstructure of the studied composites is the presence of evenly distributed particles of the SiC carbide phase against the background of a plastic aluminum matrix. In addition, the following phases occur in the microstructure: Al<sub>2</sub>O<sub>3</sub>, SiO<sub>2</sub>, Si and Al<sub>4</sub>C<sub>3</sub>.
- There were no discontinuities at the aluminum matrix-SiC particle boundary or between the SiC particles, which proves the correct selection of the SPS parameters.
- The hardness of the composite with the reinforcement phase content of 90 wt% is 2537 ± 226 HV1, while the composite with the lower reinforcement phase content (70 wt% SiC) is 286 ± 63 HV1. The relatively high hardness of the composite with the higher SiC content is due to the percentage and distribution of aluminum matrix in the microstructure of these composites.
- Increasing the share of the reinforcing phase in the form of silicon carbide from 70 to 90 wt% causes a decline in the wear resistance of the researched composites owing to chipping of the SiC particle fragments, especially at the particle boundaries of this phase.
- Increasing the pressure does not increase the wear rate of the composites with the higher content of SiC, which may result from the impact of the load on the reduction of dynamic interactions in the friction pair, affecting the cracking of the ceramic phase.
- The chipping of the strengthening phase in the composites with the higher content of SiC reduces their wear resistance.
- The wear mechanisms are mainly smearing of the aluminum matrix on the surface involved in friction, as well as cracking and chipping of SiC particle fragments, resulting from dynamic load changes in the friction pair.

**Acknowledgements** The authors would like to acknowledge Mr. Rafał Rubach (Łukasiewicz Research Network – Poznań Institute of Technology) for his support concerning the SPS process.

**Funding** Partial financial support was received from Polish State Committee for Scientific Research.

**Data and code availability** The data that support the findings of this study are available on request from the corresponding author.

## Declarations

**Conflict of interest** The authors have no financial or proprietary interests in any material discussed in this article. The authors also declared no potential conflicts of interest with respect to the research, authorship, and/or publication of this article.

**Ethical approval** This article does not contain any studies with human participants or animals performed by any of the authors.

**Open Access** This article is licensed under a Creative Commons Attribution 4.0 International License, which permits use, sharing, adaptation, distribution and reproduction in any medium or format, as long as you give appropriate credit to the original author(s) and the source, provide a link to the Creative Commons licence, and indicate if changes were made. The images or other third party material in this article are included in the article's Creative Commons licence, unless indicated otherwise in a credit line to the material. If material is not included in the article's Creative Commons licence and your intended use is not permitted by statutory regulation or exceeds the permitted use, you will need to obtain permission directly from the copyright holder. To view a copy of this licence, visit <http://creativecommons.org/licenses/by/4.0/>.

## References

1. Liu Q, Wang F, Wu W, An D, He Z, Xue Y, Zhang Q, Xie Z. Enhanced mechanical properties of SiC/Al composites at cryogenic temperatures. *Ceram Int*. 2019. <https://doi.org/10.1016/j.ceramint.2018.10.233>.
2. Gong D, Cao Y, Qian J, Chao Z, Xiu Z, Jiang L. Microstructural evolution and dimensional stability of 45vol% SiC/Al composites under long-term aging. *J Alloys Compd*. 2023. <https://doi.org/10.1016/j.jallcom.2022.168536>.
3. Zahedi A, Javadpour J, Rezaie H, Mazaheri M. The effect of processing conditions on the microstructure and impact behavior of melt infiltrated Al/SiCp composites. *Ceram Int*. 2011. <https://doi.org/10.1016/j.ceramint.2011.04.130>.
4. Hong Y, Liu J, Wu Y. The interface reaction of SiC/Al composites by spark plasma sintering. *J Alloys Compd*. 2023. <https://doi.org/10.1016/j.jallcom.2023.169895>.
5. Kang P, Zhao Q, Guo S, Xue W, Liu H, Chao Z, Jiang L, Wu G. Optimisation of the spark plasma sintering process for high volume fraction SiCp/Al composites by orthogonal experimental design. *Ceram Int*. 2021. <https://doi.org/10.1016/j.ceramint.2020.09.240>.
6. Ren S, He X, Qu X, Li Y. Effect of controlled interfacial reaction on the microstructure and properties of the SiCp/Al composites prepared by pressureless infiltration. *J Alloys Compd*. 2008. <https://doi.org/10.1016/j.jallcom.2007.01.127>.
7. Mizuuchi K, Inoue K, Agari Y, Nagaoka T, Sugioka M, Tanaka M, Takeuchi T, Tani J, Kawahara M, Makino Y, Ito M. Processing of Al/SiC composites in continuous solid–liquid co-existent state by SPS and their thermal properties. *Composites B Engineering*. 2023. <https://doi.org/10.1016/j.compositesb.2012.02.004>.

8. Kumaresan G, Arul KB. Investigations on mechanical and wear properties of Al matrix composites reinforced with hybrid SiC and Al<sub>2</sub>O<sub>3</sub> micro-particles. *Inter Metalcast*. 2023. <https://doi.org/10.1007/s40962-022-00817-6>.
9. Liu P, Wang A, Xie J, Hao S. Characterization and evaluation of interface in SiCp/Al composite. *Trans Nonferrous Met Soc China*. 2015. [https://doi.org/10.1016/S1003-6326\(15\)63740-2](https://doi.org/10.1016/S1003-6326(15)63740-2).
10. Asafa TB, Durowoju MO, Diouf S, Shongwe MB, Bayode BL, Oladosu KO, Langa T, Olubambi PA, Ismail OS, Ajala MT, Olu-kokun TO, Ibn Shamsah SM, Sadiku ER. Development, characterization and comparison of spark plasma-sintered Gr–Cu and Gr–Al composites reinforced with SiC and ZrB<sub>2</sub> particles for thermal management. *J Mater Sci: Mater Electron*. 2021. <https://doi.org/10.1007/s10854-020-05205-6>.
11. Venkatesh VSS, Deoghare AB. Microstructural characterization and mechanical behaviour of SiC and kaoline reinforced aluminium metal matrix composites fabricated through powder metallurgy technique. *SILICON*. 2022. <https://doi.org/10.1007/s12633-021-01154-9>.
12. Chintada S, Dora SP, Kare D. Mechanical behavior and metallographic characterization of microwave sintered Al/SiC composite materials – an experimental approach. *SILICON*. 2022. <https://doi.org/10.1007/s12633-021-01409-5>.
13. Mao X, Hong Y, Wang B, Liu J, Zhang Y, Feng D, Yang L, Shi C, Wu Y, Tang W. Fabrication, microstructures and properties of 50 vol.-% SiCp/6061Al composites via a pressureless sintering technique. *Powder Metall Prog*. 2017. <https://doi.org/10.1080/00325899.2017.1364895>.
14. Jafari F, Sharifi H, Reza Saeri M, Tayebi M. Effect of reinforcement volume fraction on the wear behavior of Al-SiCp composites prepared by spark plasma sintering. *SILICON*. 2018. <https://doi.org/10.1007/s12633-018-9779-2>.
15. Oliver UC, Sunday AV, Christain EIEI, Elizabeth MM. Spark plasma sintering of aluminium composites—a review. *Int J Adv Manuf Technol*. 2021. <https://doi.org/10.1007/s00170-020-06480-7>.
16. Ujah Chika O, Popoola PA, Popoola O, Uyor UO. Mechanical and thermal behaviors of Ti36-Al16-V16-Fe16-Cr16 high entropy alloys fabricated by spark plasma sintering: An advanced material for high temperature/strength applications. *J Compos Mater*. 2022. <https://doi.org/10.1177/0021998322111149>.
17. Hong Y, Wang W, Liu J, Tang W, Wu Y. Effect of porosity and interface structures on thermal and mechanical properties of SiCp/6061Al composites with high volume fraction of SiC. *Trans Nonferrous Met Soc China*. 2019. [https://doi.org/10.1016/S1003-6326\(19\)65003-X](https://doi.org/10.1016/S1003-6326(19)65003-X).
18. Sun J, Chen G, Wang B, Chen G, Tang W. Fabrication, microstructures, and properties of 50 vol.% SiCp/6061Al composites via hot pressing. *J Mater Eng Perform*. 2019. <https://doi.org/10.1007/s11665-019-04071-6>.
19. Alizadeh A, Khayami A, Karamouz M, Hajizamani M. Mechanical properties and wear behavior of Al5083 matrix composites reinforced with high amounts of SiC particles fabricated by combined stir casting and squeeze casting: A comparative study. *Ceram Int*. 2022. <https://doi.org/10.1016/j.ceramint.2021.09.093>.
20. Chen R, Iwabuchi A, Shimizu T, Seop-Shin H, Mifune H. The sliding wear resistance behavior of NiAl and SiC particles reinforced aluminum alloy matrix composites. *Wear*. 1997;213:175–84.
21. Ghosh SK, Saha P, Sutradhar G. Study of Tribological characteristics of Al-SiC metal matrix composite. *Int J Adv Mater Res*. 2015;1:53–8.
22. Smrutiranjana P, Tapan KB, Prasanta S, Goutam S. Effect of SiC weight percentage on tribological properties of Al-SiC metal matrix composites under acid environment. *J Tribol*. 2017;13:21–35.
23. Leszczyńska-Madej B, Madej M, Garbiec D. Tribological properties of spark plasma sintered Al-SiC composites. *Materials*. 2022. <https://doi.org/10.3390/ma13214969>.
24. Kare D, Chintada S, Dora SP. Damping behavior of Al/SiC composites fabricated by powder metallurgy. *SILICON*. 2022. <https://doi.org/10.1007/s12633-021-01497-3>.
25. Urena A, Martinez E, Rodrigo P, Gil L. Oxidation treatments for SiC particles used as reinforcement in aluminium matrix composites. *Compos Sci Technol*. 2004. <https://doi.org/10.1016/j.compscitech.2004.01.010>.
26. Tham L, Gupta M, Cheng L. Effect of limited matrix–reinforcement interfacial reaction on enhancing the mechanical properties of aluminium–silicon carbide composites. *Acta Mater*. 2001. [https://doi.org/10.1016/S1359-6454\(01\)00221-X](https://doi.org/10.1016/S1359-6454(01)00221-X).
27. Urena A, Escalera M, Gil L. Oxidation barriers on SiC particles for use in aluminium matrix composites manufactured by casting route: Mechanisms of interfacial protection. *J Mater Sci*. 2002. <https://doi.org/10.1023/A:1020612819045>.
28. Baker AG. Study of mechanical and physical properties for SiC/Al composites. *Int J Adv Appl Sci*. 2013. <https://doi.org/10.11591/ijaas.v2.i2.pp67-72>.
29. Leszczyńska-Madej B, Garbiec D, Madej M. Effect of sintering temperature on microstructure and selected properties of spark plasma sintered Al-SiC composites. *Vacuum*. 2019. <https://doi.org/10.1016/j.vacuum.2019.03.033>.
30. Bedir F. Characteristic properties of Al-Cu-SiCp and Al-Cu-B<sub>4</sub>Cp composites produced by hot pressing method under nitrogen atmosphere. *Mater Des*. 2007. <https://doi.org/10.1016/j.matdes.2006.01.003>.
31. Pieczonka T. Powder metallurgy processing of aluminium, *Polish Metall*. 2006–2010 Time worldwide economic crisis; 2007, pp. 37–57.
32. Pieczonka T, Kazior J. Sintering atmosphere effects on densification of Al-SiC composites. *Int Sch Sci Res Innov*. 2014;8:283–6.
33. Shaffer GB, Hall BJ. The influence of the atmosphere on the sintering of aluminium. *Metall Mater Trans*. 2001. <https://doi.org/10.1007/s11661-002-0314-z>.
34. Siddesh Kumar NG, Ram Prabhu T, Mishra RK, Eswaraprasad N, Shiva Shankar GS, Basavarajappa S. Analysis of dry sliding wear behavior of the nano composites using statistical methods with an emphasis on temperature effects. *Measurement*. 2018. <https://doi.org/10.1016/j.measurement.2018.06.064>.
35. Jerome S, Ravisankar B, Kumar Mahato P, Natarajan S. Synthesis and evaluation of mechanical and high temperature tribological properties of in-situ Al–TiC composites. *Tribol Int*. 2010. <https://doi.org/10.1016/j.triboint.2010.05.007>.
36. Abarghouie SMRM, Reihani SMS. Investigation of friction and wear behaviors of 2024 Al and 2024 Al/SiCp composite at elevated temperatures. *J Alloy Compd*. 2010. <https://doi.org/10.1016/j.jallcom.2010.04.097>.
37. Dinaharan I, Gladston JAK, Selvam JDR, Jen TCh. Influence of particle content and temperature on dry sliding wear behavior of rice husk ash reinforced AA6061 slurry cast aluminum matrix composites. *Tribol Int*. 2023. <https://doi.org/10.1016/j.triboint.2023.108406>.

**Publisher's Note** Springer Nature remains neutral with regard to jurisdictional claims in published maps and institutional affiliations.